M-56

A SHEET-CURRENT PLASMA MODEL FOR ION-CYCLOTRON WAVES*

by

Akira Hasegawa**
Electronics Research Laboratory and Department of Electrical Engineering, University of California, Berkeley, California

and

Charles K. Birdsall
Miller Institute for Basic Research in Science and Department of Electrical Engineering, University of California, Berkeley, California

*Presented in part as paper Q10, Plasma Physics Division Meeting, A.P.S., San Diego, California, Nov. 6-9, 1963.

**Present address: Bell Telephone Laboratories, Murray Hill, New Jersey.

ABSTRACT

An approximate plasma model, using current sheets, is introduced. The primary utility is to obtain the nonlinear behavior of ion-cyclotron waves. Linear analysis is used to develop the bicircular particle motion, to show the coupling of the ion-cyclotron resonance for finite $T_\perp$, to show Landau cyclotron damping for finite $T_\parallel$. The sheet model is developed in terms of vector potential $\underset{\sim}{A}$ and sheet current density $\underset{\sim}{J}_s$ for $\underset{\sim}{k}$ parallel to the steady field $\underset{\sim}{B}_o$. There are transverse fields only, with sheet motion along three coordinates. The electrons are assumed to be hot, forming a neutralizing background. The model accuracy tests show a reasonable duplication of cold plasma ion waves. The first experiment shows wave damping for $T_\parallel >> T_\perp$ at the rate expected from linear analysis, and with $T_\parallel$ decreasing, $T_\perp$ increasing. The second experiment shows wave growth for $T_\perp >> T_\parallel$, at the rate expected, and with $T_\perp$ decreasing and $T_\parallel$ increasing. The third experiment was to find the limit in $T_\perp$ for interaction with an electron stream for $\omega \sim \omega_{ci}$, the nonlinear limit found is equal transverse energies, whereas linear analysis shows an m_e/m_i smaller value. This result is encouraging for using this method for ion heating.

INTRODUCTION

The nonlinear behavior of plasmas is of great interest, for examples, in learning the ultimate state following an instability, or in finding the effectiveness of wave or beam heating processes. Linear analyses are of little help, or may even be misleading in seeking these answers. One method of solution is to condense the plasma into a managable number of super particles and to follow their motion. This approach has been used by Buneman,[1] Dawson,[2] Eldridge and Feix,[3] and others for charged sheets moving along one coordinate; in their models there were only electrostatic forces, the primary motion was that of the electrons, and the time scale was on the order of the electron plasma oscillation period. In such models, many of the results from linear analysis can be demonstrated, lending validity to the models, as well as nonlinear results previously unavailable. The indispensable tool, of course, is the high speed computer and the computer runs are essentially experiments.

In this paper a new plasma model with response to magnetic forces is given in detail. Charged sheets are used as above but are normal to a steady magnetic field $\underset{\sim}{B}_o$. The solutions are for $\underset{\sim}{k}$ parallel to $\underset{\sim}{B}_o$. The primary motion is that of the ions near the ion-cyclotron frequency. The motion, however, is in three dimensions and the fields are two dimensional. The transverse motion constitutes a sheet current and generates a magnetic field; an electric field arises from induction, but not from charge separation. The electrons are assumed to be hot, with negligible collisions and negligible transverse current in the region of interest. The electrostatic model, with potential ϕ and sheet density ρ_s coulombs/m^2 is dual with this new model with its (vector) potential $\underset{\sim}{A}$ and sheet current density, $\underset{\sim}{J}_s = \rho_o \underset{\sim}{v}_s$; the two models could be used together to obtain both electric and magnetic results. Auer, Hurwitz, and Kilb[4] have used a related model to study shocks with $\underset{\sim}{k}$ normal to $\underset{\sim}{B}$.

A special model is good only as it can duplicate results valid from other analyses. The duplication of the ion-cyclotron wave is one test. This model is also used to show ion-cyclotron Landau damping for $T_{\parallel} >> T_{\perp}$ and ion-cyclotron wave-ion-cyclotron resonance growth for $T_{\perp} >> T_{\parallel}$. The nonlinear problem of particular interest is the limit to $T_{\perp}$ attainable from interaction with an electron stream, a result of interest in ion heating. An initial estimate might equate angular momenta and show a very low limit for $T_{\perp}$ due to the low mass density of the stream; however, the result found exceeds this limit, and is equal transverse energies.

The uses of the model have only been partially exploited in this paper and serve only as an introduction to this approach. It is felt that much knowledge of large amplitude behavior of plasmas is yet to be obtained from this and related models, knowledge that is very difficult to obtain by other methods.

The paper is in three parts. Part I presents the linear analysis for ion-cyclotron waves, with a discussion of the particle motion, to show the random motion producing the ion-cyclotron resonance, to give an explicit growth rate for the ion-cyclotron wave-ion-cyclotron resonance interaction for large $T_{\perp}$, to give the Landau damping rate for large $T_{\parallel}$, and to introduce the sheet model. Part II is the development of the sheet current model; the derivation of $\underset{\sim}{A}$ is given in Appendix A and the proper force is derived in Appendix B. Part III gives the results of the computer experiments, starting with the runs for model accuracy, then the $T_{\perp} \neq T_{\parallel}$ runs and last, the stream-plasma runs.

I. LINEAR THEORY FOR CYCLOTRON WAVES

A. Dispersion Relation and Particle Motion

The electro-kinetic waves with the wave vector, $\underset{\sim}{k}$, parallel to the applied dc magnetic field, $\underset{\sim}{B}_o$, in an infinite plasma have been studied by Bernstein[5] and Harris.[6] Their dispersion relations will be used as a starting point for getting at the particle motion and coupling of waves in a warm plasma.

Let the plasma zero-order density function for the j-th species be separable, given by

$$f^j(\underset{\sim}{v}) = f^j_{\parallel}(v_z)\, f^j_{\perp}(v_x^2 + v_y^2) \quad . \tag{1}$$

Let

$$< v_z^2 > = v_T^2$$

$$< v_x^2 > = < v_y^2 > \equiv v_{T_\perp}^2 .$$

z is the direction of the dc magnetic field and the direction of the wave vector. Using the Vlasov equation and Maxwell's equations, we look for wave solutions of the first-order fields, velocities and densities. The dispersion relations for this plasma are given by the following equations (see Harris,[6] his Eqs. 29 and 30):

(a) for the longitudinal waves;

$$k^2 + \sum_j \omega_{pj}^2 \int_c \frac{\partial f^j_{\parallel}/\partial v_z}{\omega/k - v_z}\, dv_z = 0 \tag{2}$$

(b) for the transverse waves;

$$k^2c^2 - \omega^2 + \sum_j \omega_{pj}^2 \left[\int_c \frac{\omega - kv_z}{\omega - kv_z \mp \omega_{cj}}\, f^j_{\parallel}(v_z)\, dv_z \right.$$

$$\left. + \int_c \frac{(v^j_{T_\perp})^2 k^2 f^j_{\parallel}(v_z)}{(\omega - k v_z \mp \omega_{cj})^2}\, dv_z \right] = 0 . \tag{3}$$

The integration contours are to be taken above all the poles of the integrand for the transformation with the phasor $\exp -j(\omega t - kz)$. ω_{pj}, ω_{cj}; $(v_{T_\perp}^j)^2$ are the plasma frequency, the cyclotron frequency $\left[\omega_{cj} = (|e|/m_j) B_o\right]$ and $(1/2) < v_x^2 + v_y^2 >$ of j-th species, respectively.

We are interested primarily in the second equation which contains the cyclotron waves. It is known that the ion-cyclotron wave is obtained from the upper sign in Eq. (3) and is right-hand circularly polarized and that the electron-cyclotron wave is obtained with the lower sign in Eq. (3) and is left-hand circularly polarized.

As a starting place, first let us look at the waves at zero temperature in a nondrifting plasma. The dispersion relation then reduces to

$$k^2c^2 = \omega^2 + \frac{\omega\omega_{pi}^2}{\omega_{ci} - \omega} - \frac{\omega\omega_{pe}^2}{\omega_{ce} + \omega} \tag{4}$$

for the upper sign and,

$$k^2c^2 = \omega^2 + \frac{\omega\omega_{pe}^2}{\omega_{ce} - \omega} - \frac{\omega\omega_{pi}^2}{\omega_{ci} + \omega} \tag{5}$$

for the lower sign. The real ω - real k relations are plotted in Fig. 1. The $k \to 0$, $\lambda \to \infty$, frequencies ω_1 and ω_2 are generally much larger than ω_{ci}. The lower frequency velocities, $\omega \to 0$, both equations, are

$$v_p = \frac{\omega}{k} = c\left[1 + \frac{n_e m_e + n_i m_i}{\epsilon_o B_o^2}\right]^{-1/2} \equiv v_A \ ,$$

the Alfvén waves.[7] The fast waves, $v_p > c$, are primarily electromagnetic in energy and the slow waves, $v_p < v_A$, are primarily magnetokinetic. We are interested in the slow waves, especially the ion-cyclotron wave.

Now let us study the motion of the particles associated with the ion-cyclotron wave. The Eulerian equations of motion for ions in the self-consistent field which is given by Eq. (4) are, in terms of real

variables,

$$\frac{dv_{ix}}{dt} - \omega_{ci} v_{iy} = \frac{e}{m_i} E \cos(\omega t - kz)$$

$$\frac{dv_{iy}}{dt} + \omega_{ci} v_{ix} = -\frac{e}{m_i} E \sin(\omega t - kz) \qquad (6)$$

$$\frac{dv_{iz}}{dt} = 0 .$$

Similar equations exist for the electrons, obtained by changing the sign of e and ω_c. There is no drift motion to zero order in any direction, so that $d/dt = \partial/\partial t + (\underset{\sim}{v} \cdot \nabla)$ to first order omits the directional derivative, and $d/dt = \partial/\partial t$. The general solutions of these equations are easily found to be

$$v_{ix} = v^i_{o\perp} \cos(\omega_{ci} t + \theta_i) - \frac{(e/m_i)E}{\omega_{ci} - \omega} \sin(\omega t - kz)$$

$$v_{iy} = -v^i_{o\perp} \sin(\omega_{ci} t - \theta_i) - \frac{(e/m_i)E}{\omega_{ci} - \omega} \cos(\omega t - kz)$$

$$v_{iz} = v^i_{o\parallel}$$

$$v_{ex} = v^e_{o\perp} \cos(\omega_{ce} t - \theta_e) - \frac{(e/m_e)E}{\omega_{ce} + \omega} \sin(\omega t - kz) \qquad (7)$$

$$v_{ey} = v^e_{o\perp} \sin(\omega_{ce} t + \theta_e) - \frac{(e/m_e)E}{\omega_{ce} + \omega} \cos(\omega t - kz)$$

$$v_{ez} = v^e_{o\parallel}$$

$v^i_{o\perp}$, $v^i_{o\parallel}$, $v^e_{o\perp}$, $v^e_{o\parallel}$, θ_i, θ_e are given by the initial conditions, $t = 0$, of the individual particles. For a cold plasma, the individual particles have no energy in the absence of the wave so that these values are zero and remain zero. However, if the wave is applied to a hot plasma these quantities are not zero; these values must be random, in

this one dimensional model, in order to have zero net transverse current. The particles have bi-circular motion given by these equations; particles have an angular velocity ω around a center which rotates with the angular velocity ω_{ci} (or vice versa) around a fixed origin. The implication is that there is a line at $\omega = \omega_{ci}$ (and ω_{ce}) to be added to the ω - k diagrams. When a finite temperature exists in the plasma, where the wave frequency ω approaches the ion-cyclotron frequency ω_{ci}, an interference may take place between these two motions. The effect of this interaction will be studied in more detail in the next section.

These equations of motion hold for any particle. Where $v_{o\perp}$ and $v_{o\parallel}$ are zero, motion of the ions are all in phase in a plane perpendicular to z. The motion creates a convection current in the transverse direction which becomes the source of the transverse-electromagnetic field. As the velocity vector in the plane rotates to the right with angular frequency ω as can be seen from Eq. (7), the ion current on the plane also rotates in the same direction with, of course, the same angular frequency and so also the field created by it.

For the net current, the motion of the electrons must also be considered. For $\omega \lesssim \omega_{ci}$, the transmission band of the ion-cyclotron wave, the electron velocities are almost independent of ω; dropping ω compared with ω_{ce}, the particular solution coefficient is simply $-E/B_o$ so that the electron motion is an $E_{ac} \times B_o$ drift motion. The direction and the phase of this drift is the same as that of the ions. The electrons themselves may perform rotation to the left at ω_{ce}, but the centers of rotation drift together with the ions, being captured by them. Thus the ion current is reduced by the electron motion, but the ion current dominates due to the resonant denominator; the reduction is simply by ω/ω_{ci}. At very low frequencies, $\omega \ll \omega_{ci}$ the reduction is severe because the motion of the electrons and ions approach the $E_{ac} \times B_o$ drift and the

ratio of the currents at these frequencies approaches unity. However, a difference remains so there is a net current that rotates to the right, which is one of the Alfvén waves.

B. Effects of Finite and Anisotropic Temperature

Where $v_{T_\perp}$ and $v_{T_\parallel}$ are not the same, either wave growth ($v_{T_\perp} > v_{T_\parallel}$) or wave decay ($v_{T_\perp} \lesssim v_{T_\parallel}$) results. The growth, with large $v_{T_\perp}$, occurs because of the interaction between the two parts of the motion in Eq. (7). This instability has been noted by Rosenbluth[8] and by Harris.[6] The decay with large $v_{T_\parallel}$, comes about by a phase randomization along the direction of propagation. This effect is known as the cyclotron Landau damping (Stix[9]). In both situations, $v_{T_\perp} \neq v_{T_\parallel}$, the interaction tends to make the temperatures equal. The behavior will be given in sufficient detail for use in later parts. The effect of large transverse temperature will be considered first. Let us examine the dispersion relation, Eq. (3), upper sign, for $v_{T_\parallel} = 0$, which is

$$k^2 \left[1 + \frac{(v^e_{T_\perp})^2 \omega^2_{pe}}{(\omega + \omega_{ce})^2 c^2} + \frac{(v^i_{T_\perp})^2 \omega^2_{pi}}{(\omega - \omega_{ci})^2 c^2} \right] \tag{8}$$

$$= \frac{\omega^2}{c^2} \left[1 - \frac{\omega^2_{pe}}{\omega(\omega + \omega_{ce})} - \frac{\omega^2_{pi}}{\omega(\omega - \omega_{ci})} \right] .$$

The ω-k dispersion relation is sketched in Fig. 2 for real k. The electron-cyclotron slow wave is omitted. The difference between this figure and Fig. 1 is that the ion-cyclotron wave curve does not go to infinite k but terminates with the ion-resonance line at around

$$k_m \tilde{=} \sqrt{\frac{\omega_{pi}\, \omega_{ci}}{2 c\, v^i_{T_\perp}}} \tilde{=} \frac{\omega_{ci}}{v^i_{T_\perp}} \left(\frac{\beta}{8} \right)^{1/4} \tag{9}$$

$$\tilde{=} \frac{\omega_{pi}}{c} (2\beta)^{-1/4} ,$$

where β is the usual ratio of plasma to magnetic pressure. Stix[9] has given a k_{max} for $T_{\parallel} = T_{\perp}$. For $k > k_m$, ω becomes complex, with growing and decaying roots. The growth rate, $\mathrm{Im}(\omega) = \omega_i$ of the instability can be calculated from Eq. (8) and is given by the following approximate form

$$\frac{\omega_i}{\omega_{ci}} \cong \frac{\omega_{pi}^2}{2 k^2 c^2} \sqrt{\left(\frac{k}{k_m}\right)^4 - 1} \quad . \tag{10}$$

For $k \tilde{>} 1.4\ k_m$

$$\omega_i \tilde{=} \omega_{pi} \left(\frac{v_{T_\perp}^i}{c}\right)$$

independent of k and ω_{ci}. This is a relatively slow growth rate for cold plasmas but is appreciable for a hot plasma.

Now for the next step, consider the situation where there exists a finite longitudinal temperature but zero transverse temperature. The decay rate of the ion-cyclotron wave due to the longitudinal temperature can be obtained approximately in the following way. As the contributions of the electron current and the electromagnetic wave are negligible for $\omega \sim \omega_{ci}$, where the Landau damping takes place, only the ion current is considered to be the source of the wave. With this assumption and taking the distribution to be Maxwellian only in the z direction,

$$f_{\parallel}^i(v_z) = \frac{1}{\sqrt{2\pi}\ v_{T_\parallel}^i} \exp\left(-\frac{v_z^2}{2 (v_{T_\parallel}^i)^2}\right),$$

the dispersion relation becomes

$$k^2 c^2 = -\omega_{pi}^2 \left[1 - \frac{\omega_{ci}}{\sqrt{2}\, v_{T_\parallel}^i\, k} Z(\zeta)\right] \tag{11}$$

with

$$\zeta \equiv \xi + i\eta \equiv \frac{\omega - \omega_{ci}}{\sqrt{2}\, v^i_{T_{||}} k} \quad , \qquad \omega = \omega_r + j\omega_i$$

$Z(\zeta)$ is the plasma dispersion function of Fried and Conte.[10] Expanding $Z(\zeta)$ in a Taylor series of $i\eta$, following Jackson,[11] and taking only the first two terms we have

$$\eta = - \frac{\pi f(\xi)}{P\int_{-\infty}^{\infty} \frac{f'(u)}{u - \xi}\, du} \tag{12}$$

$$k^2c^2 = - \omega_{pi}^2 \left[1 - \frac{\omega_{ci}}{\sqrt{2}\, v^i_{T_{||}} k} P \int_{-\infty}^{\infty} \frac{f(u)}{u - \xi}\, du \right] \tag{13}$$

$$f(u) = \frac{1}{\sqrt{\pi}}\, e^{-u^2}$$

Eq. (13) can be used to evaluate the denominator of Eq. (12). We can obtain ω_i in the range $|(\omega_r - \omega_{ci})/(\sqrt{2}\, v^i_{T_{||}} k)| >> 1$; the Landau cyclotron damping in time is

$$\eta = - \pi \xi^2 f(\xi)$$

or, explicitly

$$\omega_i = -\sqrt{\frac{\pi}{2}}\, \frac{\omega_{ci}^2\, \omega_{pi}^4}{v^i_{T_{||}} k (k^2c^2 + \omega_{pi}^2)^2} \exp\left[- \frac{\omega_{ci}^2\, \omega_{pi}^4}{2 (v^i_{T_{||}})^2 k^2 (k^2c^2 + \omega_{pi}^2)^2} \right] . \tag{14}$$

Notice that $\mathrm{Im}(\omega)$ depends on $f(\xi)$ not on $(\partial f)/(\partial \xi)$ as is the case for the longitudinal wave (Jackson[11]).

C. Stream and Plasma Interaction

Where some component of the plasma has a drift velocity in the z direction, the dispersion relation can be obtained by appropriate

Doppler shifting of the frequency. If the entire plasma drifts, there are four kinds of forward transverse magnetokinetic waves: faster and slower electron cyclotron waves and the faster and slower ion-cyclotron waves. The polarization of these waves are left and right, and right and left respectively. For a stream to have some kind of interaction with the cyclotron waves of a stationary plasma, the polarization of the two waves should be the same. In addition, to have an instability due to the interaction, the wave in the stream should carry a negative energy (Sturrock[12]). These choices allow only two types of combination of the waves. One is the interaction between the electron slower cyclotron wave of the stream and the ion-cyclotron wave of the plasma and the other is between the ion slower cyclotron wave of the stream and the electron-cyclotron wave of the plasma.

For example, let us consider the former. The dispersion relation can be obtained from Eq. (3) by assuming the existence of three species of particles, plasma electrons and ions and the stream electrons. For a cold plasma and a stream the ω-k plot is shown in Fig. 3, for the upper sign (right-hand polarization). Solutions for growths in time, ω_i, and in distance, k_i, are shown as dashed lines. The interaction at near the ion-cyclotron frequency has been studied by Harris,[6] and Neufeld and Wright.[13] The interaction around zero frequency (time-growing only) is relatively unknown, also found by Briggs and Bers[14] independently. We call the former the cyclotron-wave instability and the latter, the Alfvén wave instability.

II. MODEL

A. Model and Corresponding Fields

The ions of the plasma have bicircular motion in a given plane at z, as was shown earlier, for a warm plasma and the ion-cyclotron wave. At a fixed t, for $k_x = 0$, $k_y = 0$, all the velocities of the particles are directed in one direction in the transverse plane and create a net current directed in the same direction, as is shown in the Fig. 4. Therefore, the phenomena can be synthesized by fixing particles on

transverse planes, and by letting the transverse planes rotate, creating a rotating transverse current. Thus the new model is called a sheet-current model. By placing a set of these transverse sheet currents along the z direction and giving them a proper phase difference plus random velocities, one can set up the cyclotron wave with finite temperature. The intention, of course, is to obtain the nonlinear behavior of the ion-cyclotron wave.

In the cyclotron waves, the electric and magnetic fields, which are created by the transverse currents, are predominantly transverse. Charge separation is assumed to be zero; the electric field is created only by the time-rate change of the magnetic flux density and thus exists only in the transverse direction. The basic equations for the fields are

$$\nabla \times \underset{\sim}{E} = - \frac{\partial \underset{\sim}{B}}{\partial t}$$

$$\nabla \times \underset{\sim}{B} = \mu_o \, J \qquad (15)$$

$$\nabla \cdot \underset{\sim}{E} = \nabla \cdot \underset{\sim}{B} = 0.$$

The source of the fields is the transverse current created by the sheets, which directly creates the magnetic field. The time rate of change of the magnetic flux density then creates the electric field. Both of these fields act to accelerate the sheets. The only field variable necessary is the magnetic vector potential $\underset{\sim}{A}$.

Let the model now consist of an infinity of the ion sheets. The motion for $k \to 0$, $\lambda \to \infty$, would have all sheets in random phase and $\omega = \omega_{ci}$ already known. The motion for large k, $\lambda <$ sheet-spacing cannot be found. Hence the motion for intermediate k, λ, is solved. The spatial behavior is assumed to be periodic of period L with N sheets in each period to be followed. The range covered is approximately $2\pi \leq kL \leq 2\pi N$ or $L/N \leq \lambda \leq L$. The restriction on having many sheets per Debye length in electrostatic models (Dawson;[2] Eldridge and Feix[3]) does not occur here. Each sheet

is made of ρ_s coulombs/m^2 and has a transverse velocity $\underset{\sim}{v}_\perp$ such that there is a sheet current $\underset{\sim}{J}_s = \rho_o \underset{\sim}{v}_\perp$ amps/m; the mass per square meter is m_s. As the charge and mass are condensed similarly from the whole volume, $\rho_s/m_s = \rho/m = e/m_i$ of the ions in question. In each period, L, it is required that the net magnetic flux, net vector potential, and net current vanish; the justification is given in Appendix A. The current in the j-th sheet is $\underset{\sim}{J}_j$ amps/m. The vector potential is then found to be (Appendix A),

$$A_x(z,t) = \frac{\mu_o}{2} \sum_{j=1}^{N} J_{jx}(t) \left\{ \left[1 - \frac{2z_j(t)}{L} \right] z - |z - z_j(t)| + \frac{[z_j(t)]^2}{L} \right\} \qquad (16)$$

and similarly for A_y. The restriction on currents are

$$\sum_{j=1}^{N} J_{jx}(t) = 0, \qquad \sum_{j=1}^{N} J_{jy}(t) = 0.$$

There is no z current, as the ions and electrons are assumed to move together along z.

The magnetic flux density $\underset{\sim}{B}(z,t)$ is obtained from $\nabla \times \underset{\sim}{A}$ as

$$B_x(z,t) = -\frac{\partial A_y}{\partial z}\bigg|_t = -\frac{A_y(t, z + \Delta z) - A_y(t,z)}{\Delta z} \qquad (17)$$

and similarly for $B_y(z,t)$. Here Δz may be any value smaller than the distance between sheets; in these calculations Δz was fixed at a value L/10 N that is, 1/10 of the uniform spacing interval, rather coarse. The value of $\underset{\sim}{B}$ to be used in the equations of motion of the j-th sheet at z_j should be the spatial average value, $(1/2)\left[\underset{\sim}{B}(z_j^+) + \underset{\sim}{B}(z_j^-)\right]$ in order to include the self force of the j-th sheet; in these calculations $\underset{\sim}{B}(z_j^+)$ was used instead, allowing for some error, diminishing as N increases.

The electric field $\underset{\sim}{E}$ is obtained from $-\left[(\partial \underset{\sim}{A})/(\partial t)\right]$ as

$$E_x(z,t) = -\frac{\partial A_x}{\partial t}\bigg|_z = -\frac{A_x(t,z) - A_x(t - \Delta t, z)}{\Delta t} \qquad (18)$$

and similarly for E_y. Δt is the integration time. Typical fields for two sheets are shown in Fig. 5.

B. Equation of Motion of Computation

The fields and currents give the acceleration of the sheets. The next step is to use these in the equations of motion to find the velocity and position a short time Δt later. With these new values, the fields are again computed and the motion again obtained, and so on. The results are made more accurate as $\Delta t \to 0$, $N \to \infty$ and as the computer program becomes more ingenious. Motion is allowed along three coordinates so there are three equations of motion; these are simply, for each sheet,

$$\begin{aligned} \frac{dv_x}{dt} &= \frac{e}{m}(E_x + v_y B_o - v_z B_y) \\ \frac{dv_y}{dt} &= \frac{e}{m}(E_y - v_x B_o + v_z B_x) \\ \frac{dv_z}{dt} &= \frac{e}{m}(v_x B_y - v_y B_x). \end{aligned} \tag{19}$$

Note that in linear analysis, the rhs of the last equation vanishes as it would be second order; it is kept here. The motion of the electrons is neglected as based on the (linear) analysis result that it contributes negligible current as $\omega \to \omega_{ci}$, the region of interest. To the order Δt, the force to be used for the interval between t and $t + \Delta t$ is calculated from

$$F \cong \frac{3}{2} F(t) - \frac{1}{2} F(t - \Delta t) \tag{20}$$

to allow for field changes during Δt, even though the sheets do not cross; the details are given in Appendix B. For example, the proper electric field to use in Eq. (19), using Eq. (18) and Eq. (20) is

$$E_x(z, t) = \frac{1}{\Delta t} \left[-\frac{3}{2} A_x(t, z) + 2A_x(t - \Delta t, z) - \frac{1}{2} A_x(t - 2\Delta t, z) \right]$$

and similarly for $\underset{\sim}{B}$. Particles leaving at $z = L$ are reinserted at $z = 0$ and vice versa.

Besides these equations, one is also interested in having the time dependence of the field and kinetic energies and of the longitudinal and transverse temperature. The energies found are really energy/m^2 of cross section, hence, energy densities. The magnetic field energy W_B is given by

$$W_B = \sum_{j=1}^{N} \underset{\sim}{J}_{sj} \cdot \underset{\sim}{A}$$

and W_{B1} shows the energy of the fundamental magnetic field, $kL = 2\pi$. The transverse kinetic energy $W_{K_\perp}$ is given by

$$W_{K_\perp} = \frac{1}{2} m_s \sum_{j=1}^{N} (v_{xj}^2 + v_{yj}^2).$$

The longitudinal temperature $T_\parallel$ is taken to be

$$\mathcal{K} T_\parallel = \frac{m_s}{N} \sum_{j=1}^{N} (v_{zj} - \langle v_{zj} \rangle)^2.$$

The $\langle\rangle$ means spatial average over the whole period. The calculation of the transverse temperature $T_\perp$, is somewhat more involved. The total transverse kinetic energy contains a coherent part W_{KC} which is associated with the coherent wave. A transverse temperature is defined by

$$\mathcal{K} T_\perp = \frac{1}{N} (W_{K_\perp} - W_{KC}).$$

W_{KC} is obtained from the wave energy in terms of the magnetic field, which is Fourier analysed,

$$W_{KC} = \frac{1}{2} \frac{m_s k_1^2}{e^2 n \mu_o^2} \sum_{p=1}^{P} p^2 B_{xp}^2$$

where B_{xp} is the amplitude of the p-th spatial harmonic of the transverse magnetic field; the coherent part is arbitrarily chosen to be the first 8 harmonics, $P = 8$. The above relation is obtained from $\nabla \times \underset{\sim}{B} = \mu_o \underset{\sim}{J} = \mu_o n e \underset{\sim}{v}$; it was assumed that the density variation with z was negligible which is true in the linear region but may not be so here.

An energy correction is used in order to reduce the effect of errors. After each step the total energy is calculated and the fields squared and velocity squared are adjusted by any change. For the largest part of most runs, the correction is small.

III. APPLICATION AND RESULTS

A. Trial Runs

About twenty test runs were made before more sophisticated problems were tried. The aim was to find the relation between the error and the number of sheets per period, N, and the integration time Δt. The first runs were with $kL = 2\pi$ at small amplitude, zero temperature, with initial uniform sheet spacing. Wave amplitude error was found to be sensitive to N and Δt, increasing as $\Delta t/N$. However, the phase velocity error was not sensitive to these parameters and almost did not appear to change in the range of at least $10 \leq N \leq 60$ and $0.01 \leq (\Delta t)/(\tau_c) \leq 0.05$; $\tau_c = 1/\omega_{ci}$. The phase velocity was obtained from the velocity of the zero crossings of the wave. For example, the amplitude error which was less than a percent for $N = 60$ and $(\Delta t)/(\tau_c) = 0.01$, becomes a few percent for the case $N = 10$ and $(\Delta t)/(\tau_c) = 0.03$, in the time necessary for the wave to propagate one period. On the other hand, the error in phase velocity was found to be almost constant and less than a percent for these ranges of N and Δt, as shown in Fig. 6. It should be noted that this problem is somewhat more complex than that of one-dimensional charged sheets and uses considerable more computer time per significant run. Hence, there are, to date, relatively fewer runs and coarser results.

B. Effect of Anistropic Temperature

Linear analysis shows that $T_\perp \neq T_\parallel$ will lead to growth or decay of the wave. The purpose of this section is to demonstrate these phenomena with the model and observe the change of the temperature, not available from linear analysis as it is a zero-order quantity.

First we consider the effect of the longitudinal temperature. The experiment was done by adding some initial random longitudinal velocity to the sheets in addition to the set of initial conditions which was discussed in the previous section (wave, with transverse velocities only). The random velocities were chosen from the cumulative Maxwell distribution by giving a uniformly distributed set of random numbers between one and zero to the distribution and picking up the corresponding random variables. Therefore, the initial velocities are supposed to have a Maxwell distribution in the ensemble set of particles per one wave length. The random energy was less than one percent of the wave energy. The results of the experiment No. 1 are shown in Fig. 7. The parameters are shown in Table 1. There is decay of the fundamental Fourier mode and the total magnetic field energy. The decay rate matches quite well with the linear theory (which assumes constant temperature) obtained from Eq. (14); the longitudinal temperature used to calculate the decay rate is the value at $\omega_{ci}t = 8$. The longitudinal temperature is not constant but decays with about the same decay rate as the field energy. Some of these energies appear to be converted to transverse kinetic energy which increases with time, implying a growth of transverse temperature. A plot (not shown) of the transverse kinetic energy of each sheet does show a growth of the variance. Hence with $T_\parallel$ decreasing, $T_\perp$ increasing, there appears to be an entropy increase and tendency toward an isotropic temperature.

For the second experiment, consider the effect of the transverse temperature. A random transverse velocity with a Maxwell distribution was given to each sheet initially in addition to the transverse-wave velocity. The results of the experiment are shown in Fig. 8.

The initial transverse temperature was chosen so that the wave number of the initially excited wave is $k > k_m$, the critical wave number for the growth of the wave. Notice the growth of the fundamental Fourier mode of the magnetic field. The linear result shown was calculated using Eq. (19) assuming that the growing and decaying waves were equally excited. Another experiment, not shown here, for $k < k_m$, showed no growth of the fundamental wave but showed growth of the total field energy and of the higher harmonics which were created both from the fundamental by nonlinearity and the above growth mechanism.

The longitudinal temperature is seen to grow (from zero) initially much faster than the wave. This growth appears to be physically consistent. The wave energy grows at the expense of the transverse temperature, by conversion of random energy to coherent energy. This alone is contrary to H theorem-like arguments. However the growth of the wave is possible and entropy can increase if accompanied by a growth of the longitudinal temperature.

C. Electron Stream-Plasma Interaction

An electron stream may interact with the plasma ions near ω_{ci} as known from linear analysis. The interest is to obtain the growth of the ion-transverse temperature due to the interaction. The real k model is used with the implication that the measurements are made in the center part of a finite plasma, considerably removed from the boundary and from an external source for the electrons. A set of experiments have been done and the growth rate in time of the wave has matched very well with that of the linear analysis. In the region (in time) of linear interaction, it was found that (subscript b is for stream)

$$\frac{v_{i_\perp} m_i \sqrt{n_i}}{v_{b_\perp} m_b \sqrt{n_b}} \simeq 1$$

which can be derived also from the linear analysis. This result is discouraging if the object is to increase $v_{i_\perp}$, for then the ratio of transverse energies is

$$\frac{m_i(v_{\perp i})^2}{m_b(v_{\perp b})^2} \cong \frac{m_b n_b}{m_i n_i} .$$

This is generally small due to both the mass ratio and density ratio of stream electrons to plasma ions. However, the nonlinear results are considerably more encouraging, as will be seen.

The results of a trial in the nonlinear region are shown in Figs. 9-12 for experiment No. 3. Fig. 9 shows the development of the ion-transverse kinetic energy and the stream transverse kinetic energy. The ratio of these energies is about 1/5 up to the time where the nonlinear interaction starts ($\omega_{ci}t \cong 18$). Beyond this time both kinetic energies tend to grow with almost the same rate until $\omega_{ci}t \cong 40$, when the stream kinetic energy decreases rapidly, giving part of its energy to the ion-kinetic energy. However, most of this goes to the longitudinal energy causing reflection (negative velocity) of the stream, as can be seen by the plot of the longitudinal velocities of the sheets in Fig. 10. In this figure one can see that four out of the ten sheets nearly stop at $\omega_{ci}t \cong 40$ where the stream transverse kinetic energy becomes maximum. Beyond this time these four sheets are reflected. Fortunately at longer times the transverse-ion kinetic energy becomes the same as the stream transverse kinetic energy exceeding the small linear analysis limit. In Fig. 11 are shown transverse temperatures of the ions and stream with the magnetic field energy. The field energy and the stream temperature grow exponentially in the linear interaction region where the ion temperature grows more slowly; however, the latter continues to grow in the nonlinear interaction region. The large decay of the field energy in the nonlinear region is possibly due to the cyclotron Landau damping. The transverse kinetic energy of each ion sheet is plotted in Fig. 12. Some of the sheets show almost no growth, while the others show a large growth. The gross result is that the nonlinear limit of $v_{\perp i}$, with roughly equal transverse energies,

substantially exceeds the linear analysis result (down by the density ratio) lending real hope to this means of ion heating.

It would be desirable to resolve this experiment as a semi-infinite plasma with a stream injected from one side, to observe the growth in distance as well as time.

CONCLUSIONS, DISCUSSION

A new sheet-current model, useful for warm plasmas and $\omega \sim \omega_{ci}$ has been shown to duplicate with reasonable accuracy known results for $T = 0$. The cyclotron wave damping for $T_{\parallel} >> T_{\perp}$ and the growth for $T_{\perp} >> T_{\parallel}$ appear also in reasonable agreement. The electron stream-ion interaction, a possible means for ion heating, in the nonlinear limit exceeds the limit of the linear analysis, lending encouragement for use of this mechanism.

The initial model development has been introductory, not without approximations and with only a small number of experiments. There is need for refinement and for greater breadth of applications, to satisfy the real need for nonlinear solutions. (Readers needing greater detail than given here should consult Ref. 15.)

ACKNOWLEDGMENTS

The help of Mrs. Gail Nirdlinger in computer programming is gratefully acknowledged.

The authors are grateful for the support of Aeronautical Systems Division Contract AF 33(657)-7614/AF 33(615)-1078 and of joint Tri-Service support, Contract AF-AFOSR-139-63 and to the Charles F. Kettering Foundation for making available some of the computer time used in this work.

APPENDIX A

Calculation of $\underset{\sim}{A}$

The vector potential $\underset{\sim}{A}$ may be obtained by integrating $\nabla \times \underset{\sim}{A} = \underset{\sim}{B}$, as $\underset{\sim}{B}$ is easily found for sheet currents, or by integrating

$$\underset{\sim}{A}(\underset{\sim}{r}, t) = \frac{\mu_o}{4\pi} \int_v \frac{\underset{\sim}{i}(\underset{\sim}{r}', t)\, dV'}{|r - r'|} = \frac{\mu_o}{4\pi} \int_{\text{all sheets}} \frac{J_s'\, dx'\, dy'}{|r - r'|}$$

In the former, $\underset{\sim}{A}$ is determined to within a function of time $c(t)$ and in the latter, to within $\nabla\psi$; these functions are obtained from enforcing the boundary and periodicity requirements. It is instructive to use parts of both methods, partly to become familiar with the model (the Coulomb force electrostatic model is much simpler) and to expose the pitfalls.

The conditions imposed or implied by the model are:

(i) at a sheet of thickness $z^+ - z^- = \zeta \longrightarrow 0$,

$$B_x(z^+) - B_x(z^-) = \mu_o J_y\,, \quad -B_y(z^+) + B_y(z^-) = \mu_o J_x, \quad \underset{\sim}{A}(z^+) = \underset{\sim}{A}(z^-)$$

(ii) over the enitre model, all periods

$$\int \underset{\sim}{J} \cdot d\underset{\sim}{S} = 0 \quad \text{or} \quad \sum_{\text{all sheets}} J_x = 0, \quad \sum_{\text{all sheets}} J_y = 0$$

The implication is that at large radial distance, away from the region of calculation, the sheets with +x directed currents are electrically connected to those with -x directed currents, forming the necessary closed loop. As all periods are alike, the sums are taken over one period, N sheets.

(iii) over the entire model, all periods

$$\int \underset{\sim}{B} \cdot d\underset{\sim}{S} = 0, \quad \int \underset{\sim}{E} \cdot d\underset{\sim}{S} = 0, \quad \int \underset{\sim}{A} \cdot d\underset{\sim}{S} = 0.$$

The fields $\underset{\sim}{B}$, $\underset{\sim}{E}$, and $\underset{\sim}{A}$ are transverse to z so that the areas $d\underset{\sim}{S}$ are dzdy and dzdx; however, there are no variations with x or y so that for the general field $\underset{\sim}{G}$,

$$\int G_x \, dz = 0, \quad \int G_y \, dz = 0 \ .$$

As periods are alike, the integrals are taken over one period, $0 \leq z < L$. One finds from the periodicity requirement, $\underset{\sim}{A}(0,t) = \underset{\sim}{A}(L,t)$, that the above integrals over $\underset{\sim}{B}$ are satisfied.

From integration over the sheets, one has

$$\underset{\sim}{A} = \frac{\mu_o}{2} \sum_{j=1}^{N} \underset{\sim}{J}_{sj} \ z_n$$

where z_n is the distance from the j^{th} sheet to the observer at z,

$$z_n = - |z - z_j| \ .$$

However, in treating one isolated period, separated (physically) from all others, one must be careful of what can occur at the boundaries, $z = 0, L$, as these planes are shared by adjacent periods. That is, there generally is no net current at these planes, but split in half, there may be currents. These currents are equal and opposite and provide a uniform $\underset{\sim}{B}(t)$; the contribution to $\underset{\sim}{A}$ is easily found to be

$$\frac{\mu}{2} \ J_{wall} \ (2z - L)$$

where $J_{wall} = J_{wall}(t)$. The $\underset{\sim}{A}$ found so far contains all but $c(t)$. Requiring that $\int_0^L A \, dz = 0$ gives $c(t)$ (for each component),

$$c(t) = \frac{\mu}{2} \sum_{j=1}^{N} J_j \left(\frac{z_n^2}{L} + \frac{L}{2} - z_n \right)$$

and using $\underset{\sim}{A}(0,t) = \underset{\sim}{A}(L,t)$ gives $\underset{\sim}{J}_{wall}$,

$$\underset{\sim}{J}_{wall}(t) = \sum_{j=1}^{N} \underset{\sim}{J}_j (L - 2 \ z_n) \ / 2L \ .$$

Adding all terms produces Eq. (16).

APPENDIX B

Calculation of Force

In contrast with the electrostatic sheet problem, where the force on a sheet is constant until it crosses another sheet, here the forces change within the integration period Δt even without crossings. Consider the force as $F(t, z)$ at time t, sheet position z; at time $t + \delta t$, the sheet will be at $z + \delta z$ and the force will be $F(t + \delta t, z + \delta z)$. The two forces are related by

$$F(t + \delta t, z + \delta z) = F(t, z) + \frac{dF}{dt}\,\delta t + \frac{d^2F}{dt^2}\,\frac{(\delta t)^2}{2!} + \cdots \qquad (B.1)$$

where δz is related to δt by $v_z \delta t = \delta z$, and F is then the force at the sheet position, as desired. For machine calculation, it is convenient to have one value of force to use during the machine time step Δt, such that the change in velocity of the sheet being followed, Δv is obtained simply from

$$\Delta v = F \Delta t. \qquad (B.2)$$

Should the F here be $F(t, z)$ or $F(t + \Delta t, z + \Delta z)$ or some value in between such as the average of these two? The velocity at the end of Δt is similarly

$$v(t+\Delta t, z + \Delta z) = v(t, z) + \frac{dv}{dt}\Big|_t \Delta t + \frac{d^2v}{dt^2}\Big|_t \frac{\Delta t^2}{2!} + \cdots$$

which is seen to be

$$= v(t, z) + F\Big|_t \Delta t + \frac{dF}{dt}\Big|_t \frac{\Delta t^2}{2!} + \cdots \quad . \qquad (B.3)$$

That is, the change in velocity is

$$\Delta v = v(t + \Delta t, z + \Delta z) - v(t, z)$$

$$= \left[F\Big|_t + \frac{dF}{dt}\Big|_t \frac{\Delta t}{2!} + \frac{d^2F}{dt^2}\,\frac{(\Delta t)^2}{3!} + \cdots \right] \Delta t \qquad (B.4)$$

$$= F(t + \Delta t/2)\, \Delta t,$$

keeping the first two terms. Substituting $\delta t = \Delta t/2$

into Eq. (B. 1) and putting into Eq. (B. 4), it is also seen that F in Eq. (B. 2) is then the average of the forces at the start and finish of the interval or force at the median time, $t + \Delta t/2$. Hence, we will use

$$\Delta v = \left[F(t, z) + \frac{dF(t, z)}{dt} \quad \frac{\Delta t}{2} \right] \Delta t . \qquad \text{(B. 5)}$$

The derivative will be evaluated from the previous step as

$$\frac{dF}{dt} = \frac{F(t, z) - F(t - \Delta t, z - \Delta z)}{\Delta t}$$

so that

$$\Delta v = \left[\frac{3}{2} F(t, z) - \frac{1}{2} F(t - \Delta t, z - \Delta z) \right] \Delta t.$$

One asks about keeping the higher order terms in order to evaluate the error; use $\delta t = \Delta t/2$ in Eq. (B. 1) and put into Eq. (B. 2) and subtract from Eq. (B. 4) to obtain

$$\Delta v\Big|_{(B.\,4)} - \Delta v\Big|_{(B.\,2)} = \frac{d^2F}{dt^2} \frac{(\Delta t)^3}{24} + 0\,(\Delta t^4). \qquad \text{(B. 6)}$$

This further correction, even for $F'' \sim F'$, is $\Delta t/12$ smaller than the first correction used in Eq. (B. 5) and hence is made vanishingly small by making Δt small.

REFERENCES

1. O. Buneman, "Dissipation of currents in ionized media," Phys. Rev. 115, No. 3, 503 (1959).
2. J. Dawson, "One dimensional plasma model," Phys. Fluid 5, No. 4, 445 (1962).
3. O. C. Eldridge and M. Feix, "One-dimensional plasma model at thermodynamic equilibrium," Phys. Fluid 5, No. 9, 1076 (1962).
4. P. L. Auer, H. Hurwitz, Jr., and R. W. Kilb, "Low mach number magnetic compression waves in a collision free plasma," Phys. Fluid 4, No. 9, 1105 (1961).
5. I. B. Bernstein, "Waves in a plasma in a magnetic field," Phys. Rev. 109, No. 1, 10 (1958).
6. E. G. Harris, "Plasma instabilities associated with anisotropic velocity distributions," J. Nucl. Energy, Pt. C; Plasma Phys. 2, 138 (1961).
7. H. Alfvén, "On the existence of electromagnetic hydrodynamic waves," Arkiv. Math. Ast. Phys. 29B, 2 (1942).
8. M. N. Rosenbluth, Bull. Amer. Phys. Soc. 114, 197 (1959).
9. T. H. Stix, The Theory of Plasma Waves (McGraw-Hill Book Co., Inc., New York, 1962).
10. B. D. Fried and S. D. Conte, The Plasma Dispersion Functions (Acad. Press, New York, 1961).
11. J. D. Jackson, "Longitudinal plasma oscillations," J. Nucl. Phys., Pt. C; Plasma Phys. 1, 171 (1960).
12. P. A. Sturrock, "Kinematics of growing waves," Phys. Rev. 112, No. 12, 1488 (1958).
13. J. Neufeld and H. Wright, "Instabilities in a plasma-beam system immersed in a magnetic field," Phys. Rev. 129, No. 4, 1489 (1963).
14. R. J. Briggs and A. Bers, "Electron beam interaction with ions in a warm plasma," Proc. of Fourth Symposium on the Engineering

Aspects of Magnetohydrodynamics, Univ. of Calif., Berkeley, California (1963).

15. A. Hasegawa and C. K. Birdsall, "Plasma heating by injection of charged particles," Electronics Research Laboratory Technical Report 64-5 University of California, Berkeley, California (March 1964).

LIST OF ILLUSTRATIONS

Fig. 1. Dispersion (or ω - k) diagram for cold plasma, for waves transverse to $\underset{\sim}{B}_o$, from Eq. (4), solid line and from Eq. (5), dashed line.

Fig. 2. Dispersion diagram for transverse waves in a warm plasma, $T_\perp \neq 0$, $T_\parallel = 0$, ion waves only.

Fig. 3. Dispersion diagram for cold plasma and electron stream for right-hand polarization.

Fig. 4. Charged sheet in steady field B_o for use in nonlinear calculations.

Fig. 5. Magnetic field B_x and corresponding vector potential A_y for two sheets in periodic model, period L.

Fig. 6. Comparison of phase velocity v_p obtained from linear analysis and sheet model for varying number of sheets N, integration period Δt, and incremental distance $\Delta z/L$ used to obtain $\partial \mathbb{A}/\partial z$. The solid line is the linear analysis result. The values used are tabulated below; for all runs $\Delta z/L = 0.01$.

	$\frac{kc}{\omega_{ci}}$	$\left(\frac{\omega_{pi}}{\omega_{ci}}\right)^2$	N	$\frac{\Delta t}{\tau_c}$
(a)	1.5	1	20	0.03
(b)	1.75	1	20	0.03
(c)	5.0	10	20	0.03
(d)	8.99	10	60	0.05

Fig. 7. Change of field and kinetic energies and $T_\parallel$ with time. $T_\perp = 0$ initially. Experiment 1.

Fig. 8. Change of field energy and $T_\parallel$ with time for an initial $T_\perp$. $T_\parallel = 0$ initially. Experiment 2.

Fig. 9. Change of ion and stream transverse kinetic energies with time; decrease in average stream velocity. k chosen to give maximum Im ω. Experiment 3.

Fig. 10. Stream sheet axial velocities for Experiment 3.

Fig. 11. Transverse ion and stream temperatures and total field energy. Experiment 3.

Fig. 12. Ion sheet transverse energies for Experiment 3.

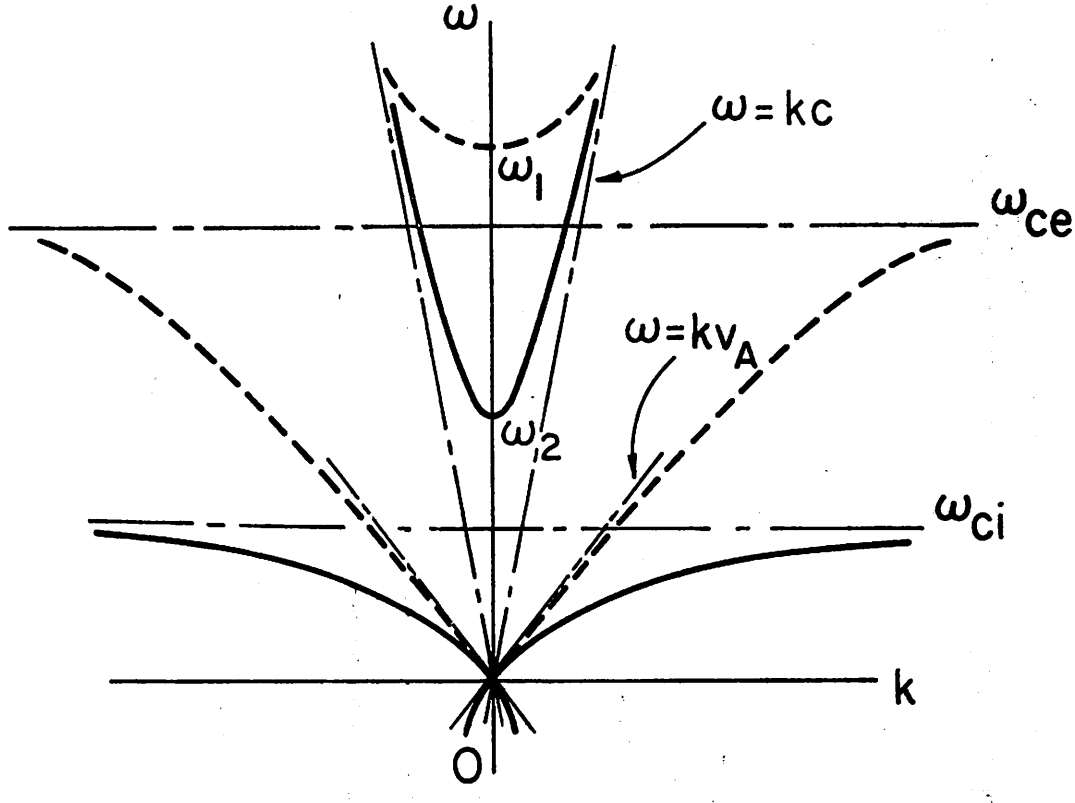
ω
ω = kc
ω1
ωce
ω = kvA
ω2
ωci
k
0

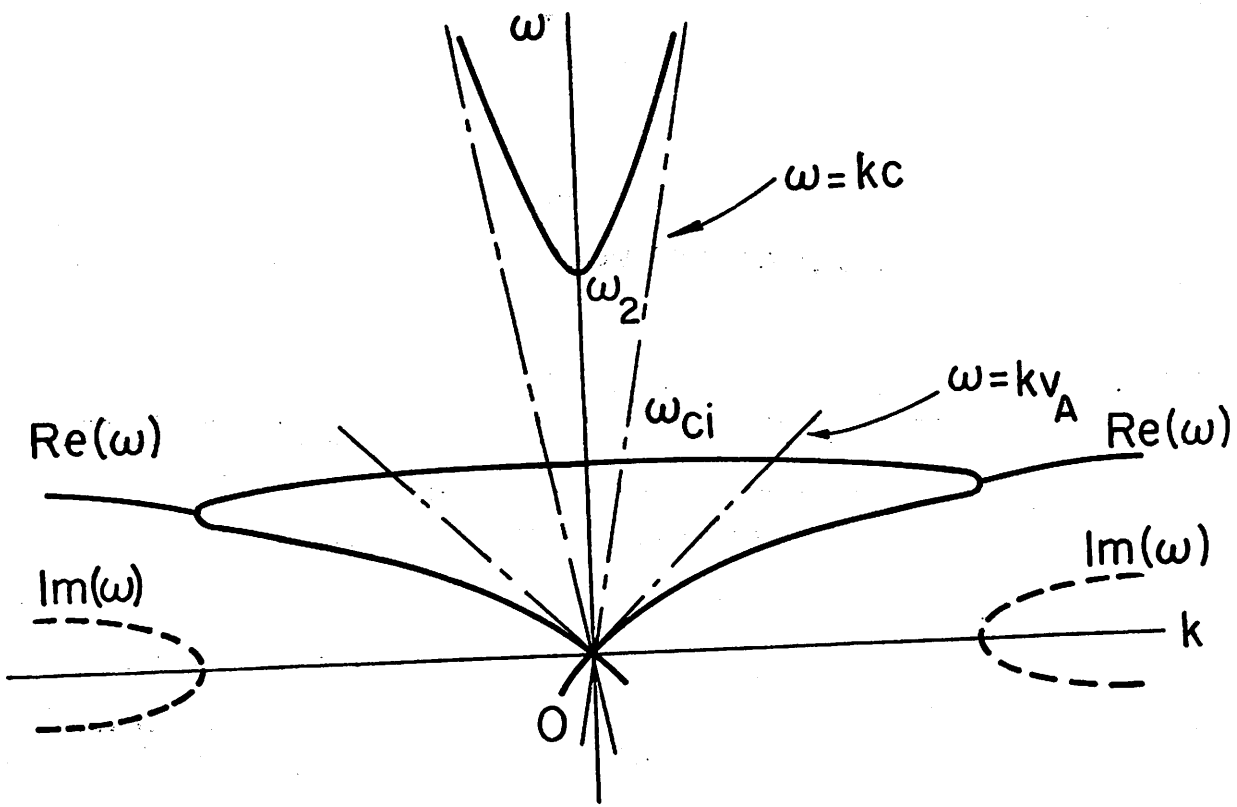
ω
ω=kc
ω2
ωci
ω=kvA
Re(ω)
Re(ω)
Im(ω)
Im(ω)
k
0

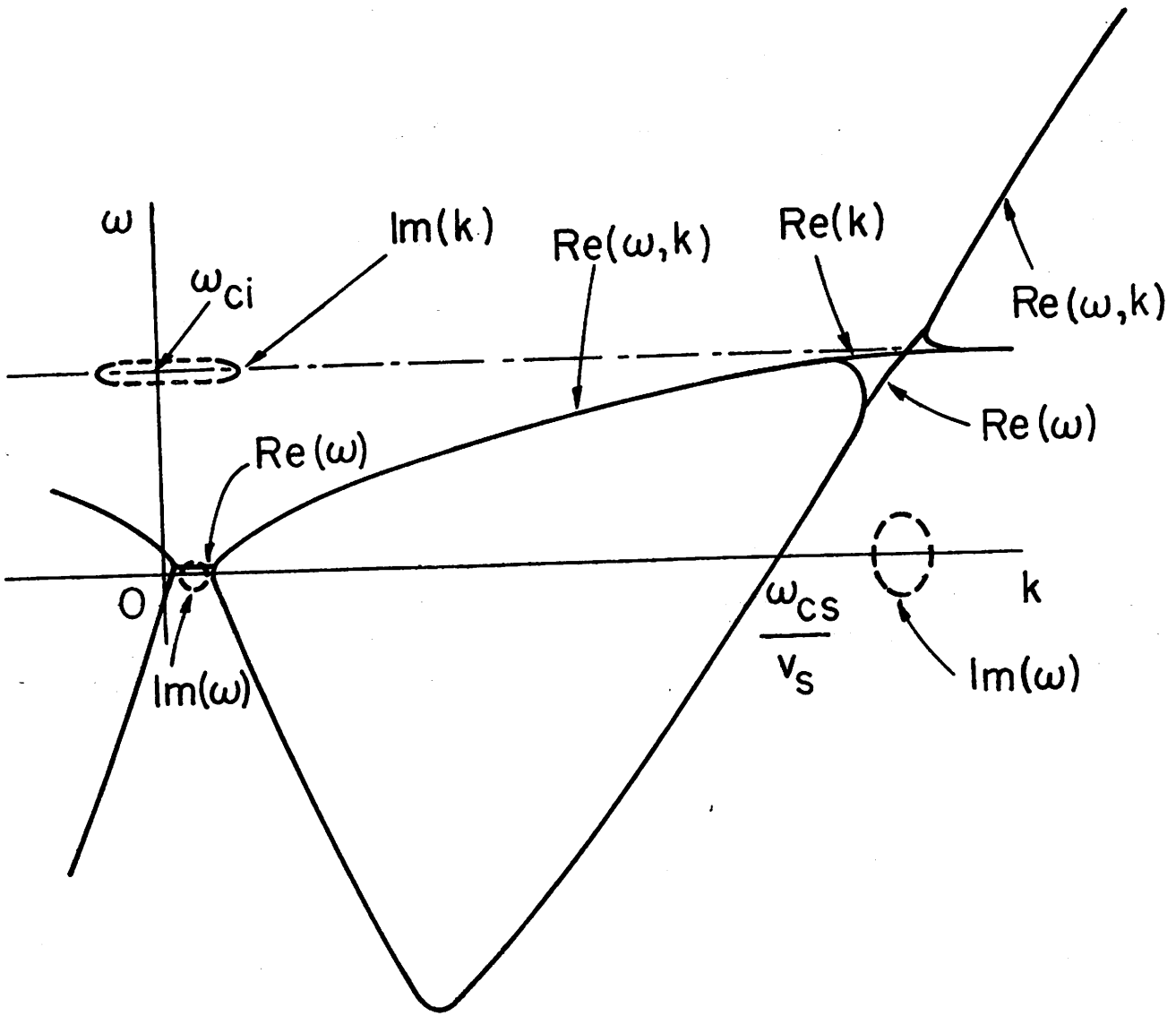
ω
Im(k)
Re(ω,k)
Re(k)
Re(ω,k)
ωci
Re(ω)
Re(ω)
O
k
ωcs
vs
Im(ω)
Im(ω)

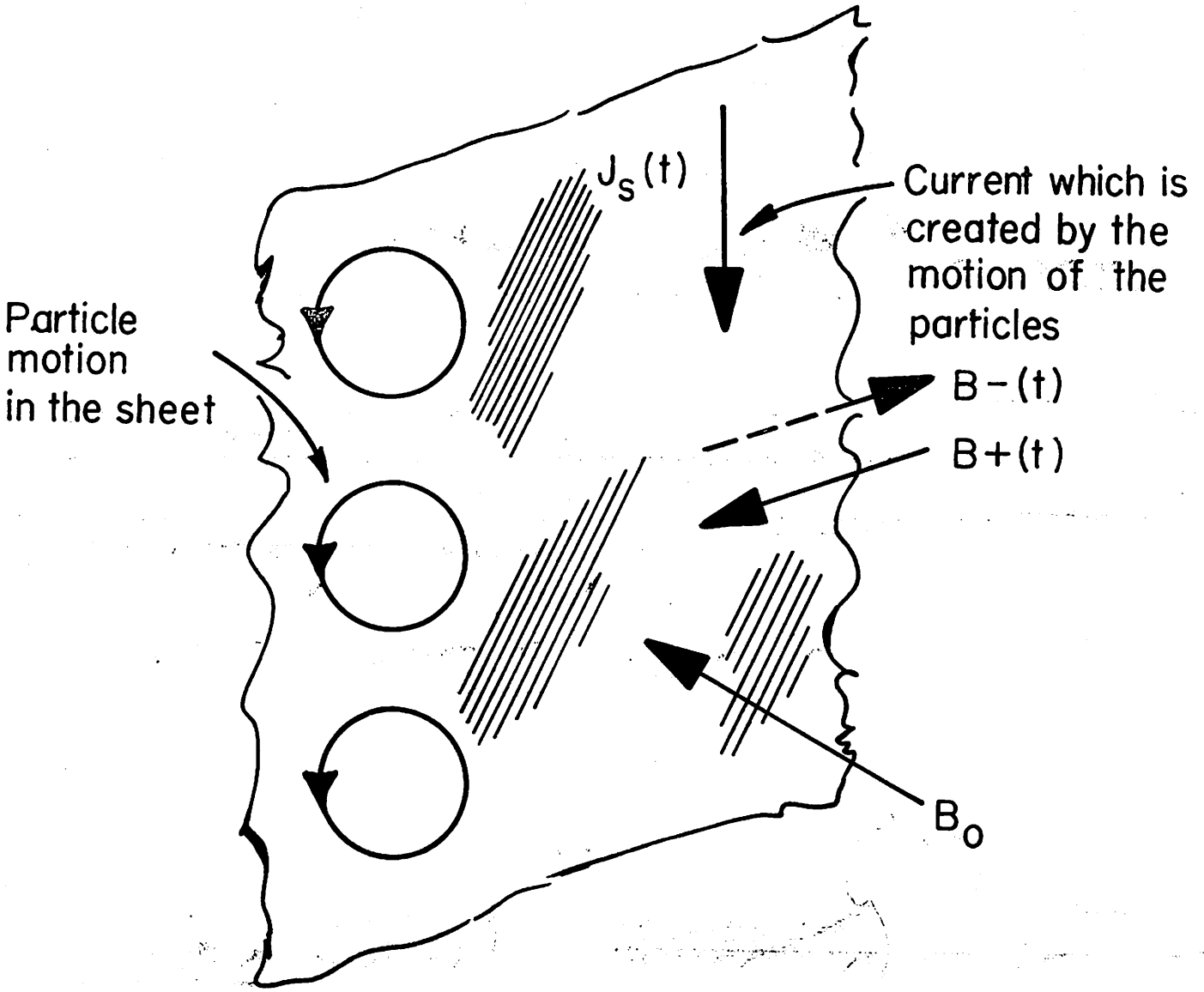
$J_s(t)$
Current which is created by the motion of the particles
Particle motion in the sheet
B−(t)
B+(t)
B_o

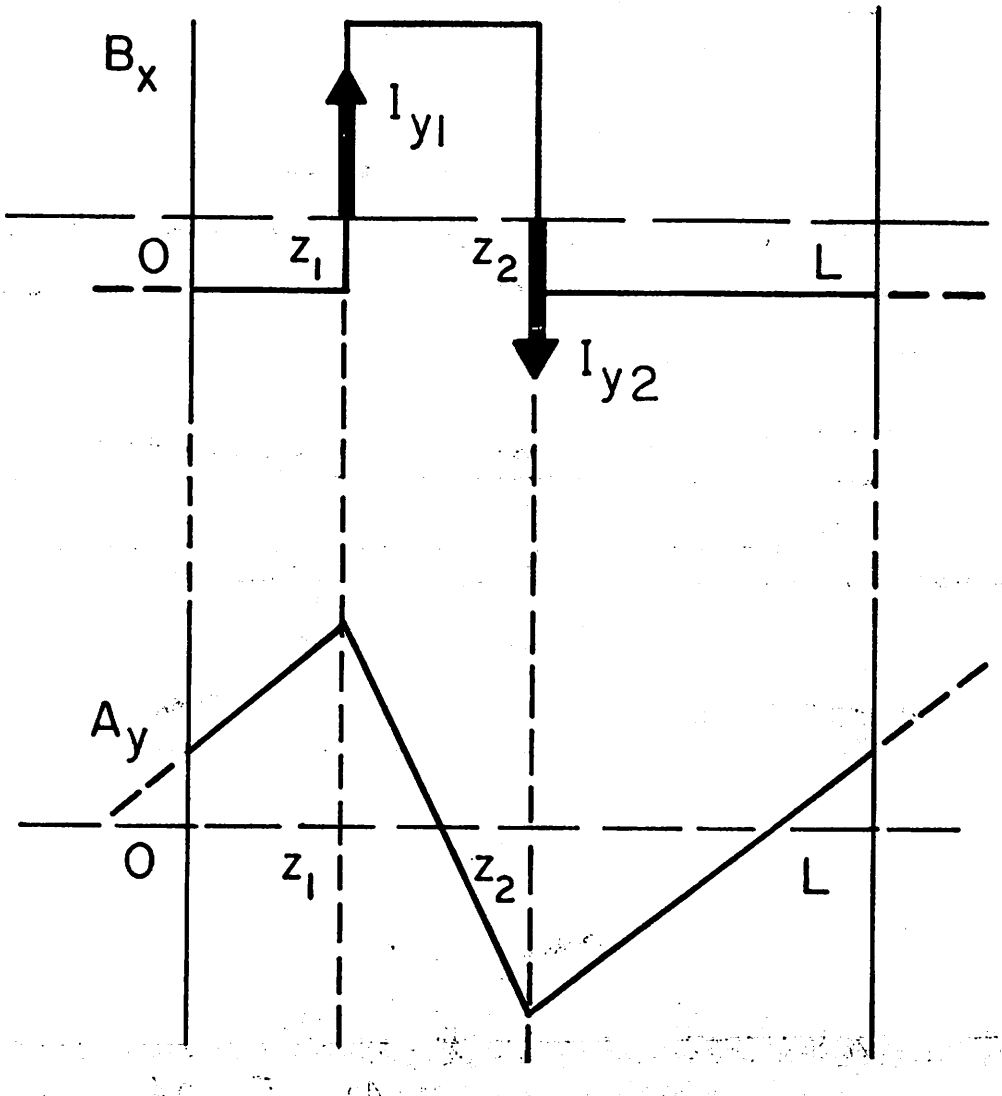
B_x
I_{y1}
0
z_1
z_2
L
I_{y2}
A_y
0
z_1
z_2
L

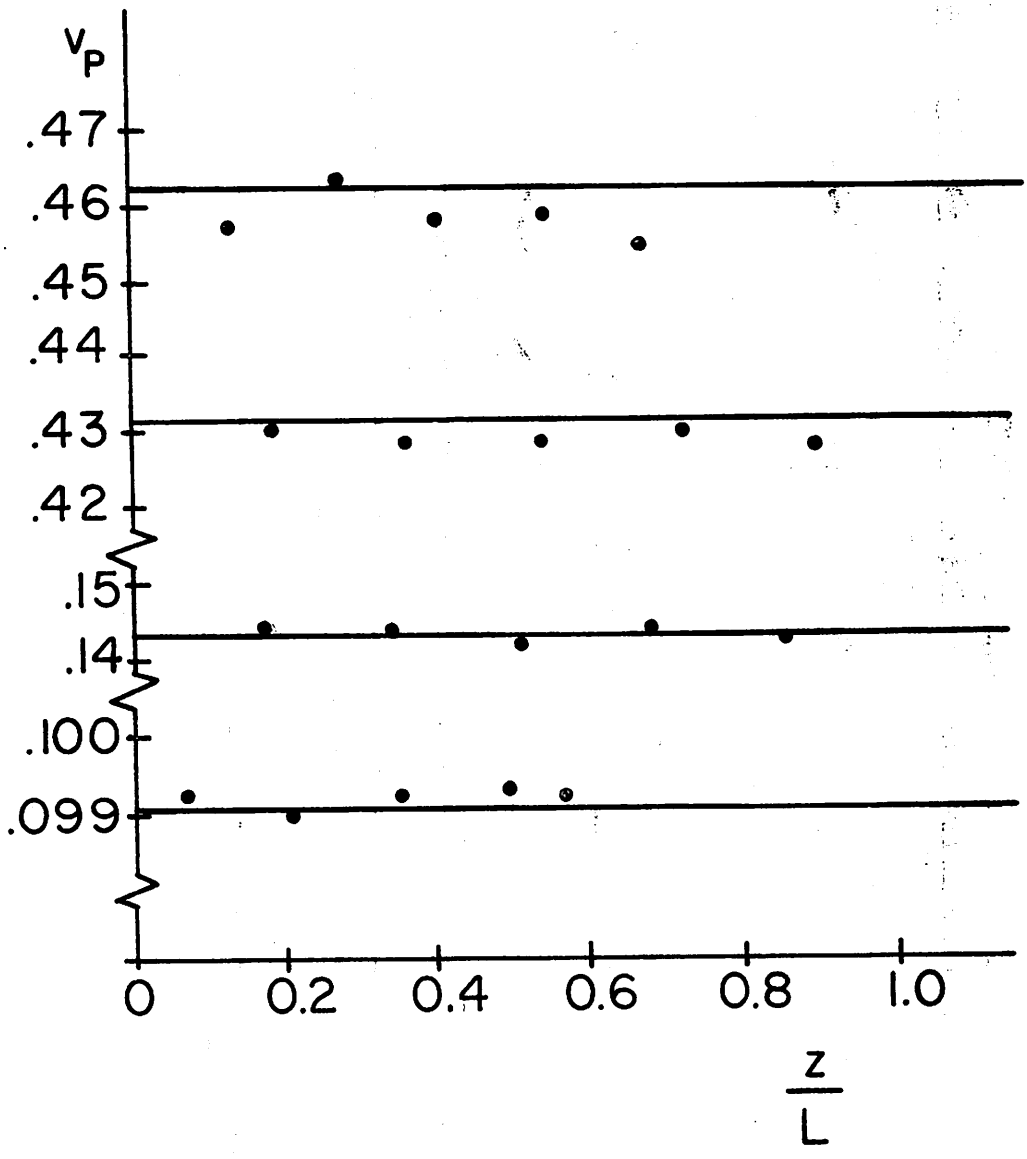
v_p
.47
.46
.45
.44
.43
.42
.15
.14
.100
.099
0
0.2
0.4
0.6
0.8
1.0
$\frac{z}{L}$

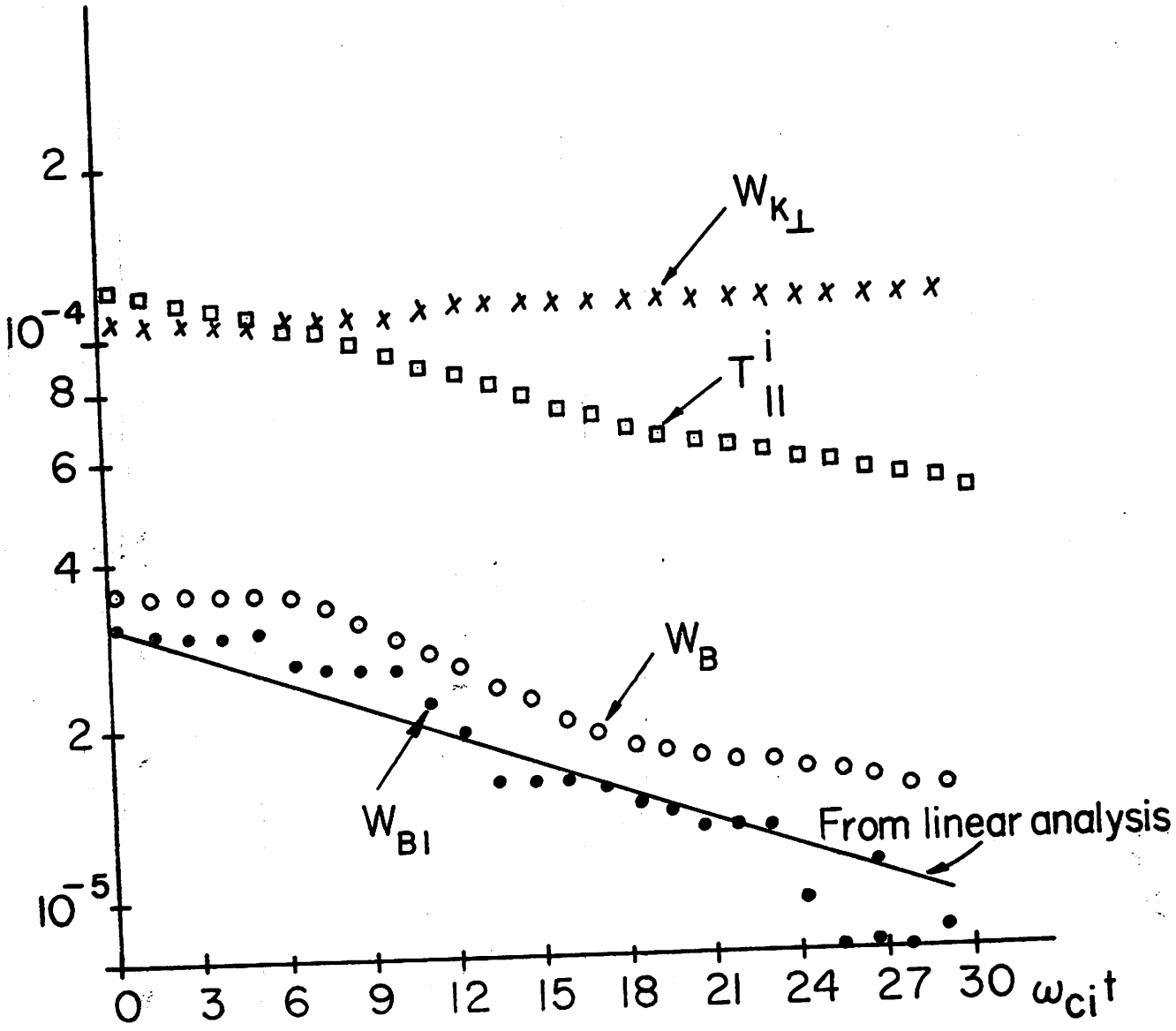
2
10^{-4}
8
6
4
2
10^{-5}
$W_{K_\perp}$
$T_{\parallel}^{i}$
W_B
W_{BI}
From linear analysis
0
3
6
9
12
15
18
21
24
27
30
$\omega_{ci}t$

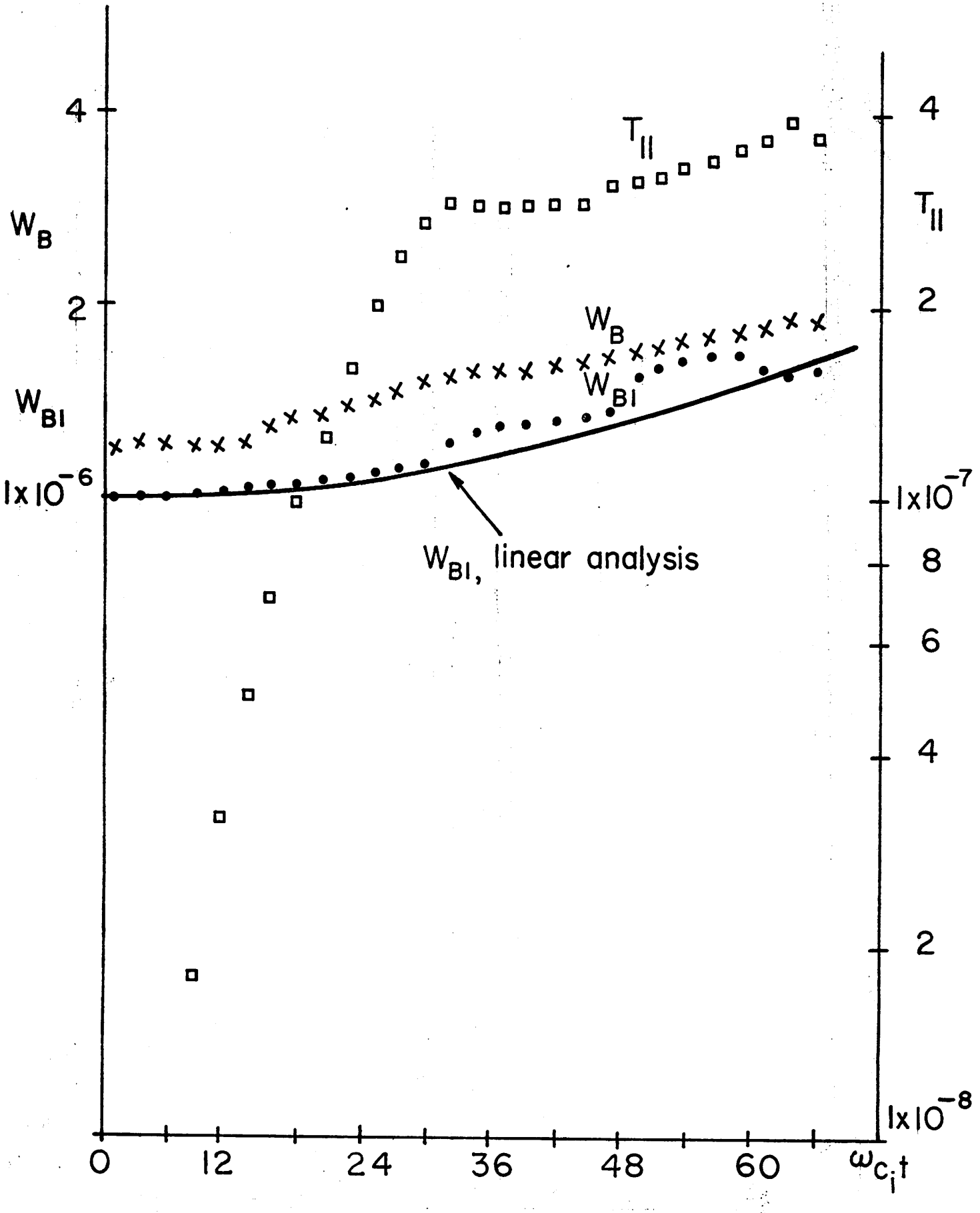
4
2
W_B
W_{BI}
$1x10^{-6}$
T_{II}
W_B
W_{BI}
W_{BI}, linear analysis
4
T_{II}
2
$1x10^{-7}$
8
6
4
2
$1x10^{-8}$
0
12
24
36
48
60
$\omega_{c_i}t$

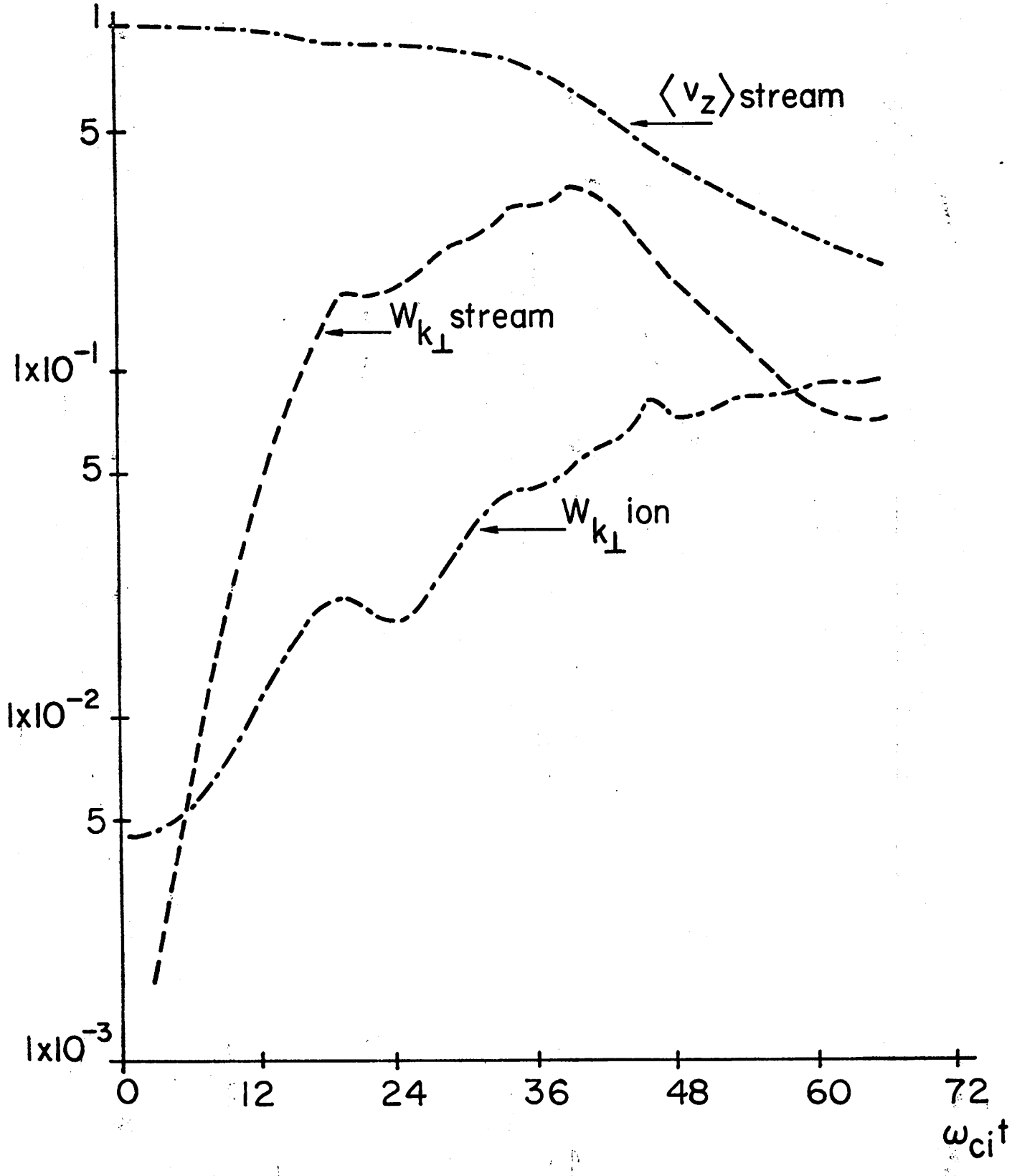
1
5
1x10^-1
5
1x10^-2
5
1x10^-3
⟨v_z⟩stream
W_k⊥ stream
W_k⊥ ion
0
12
24
36
48
60
72
ω_ci t

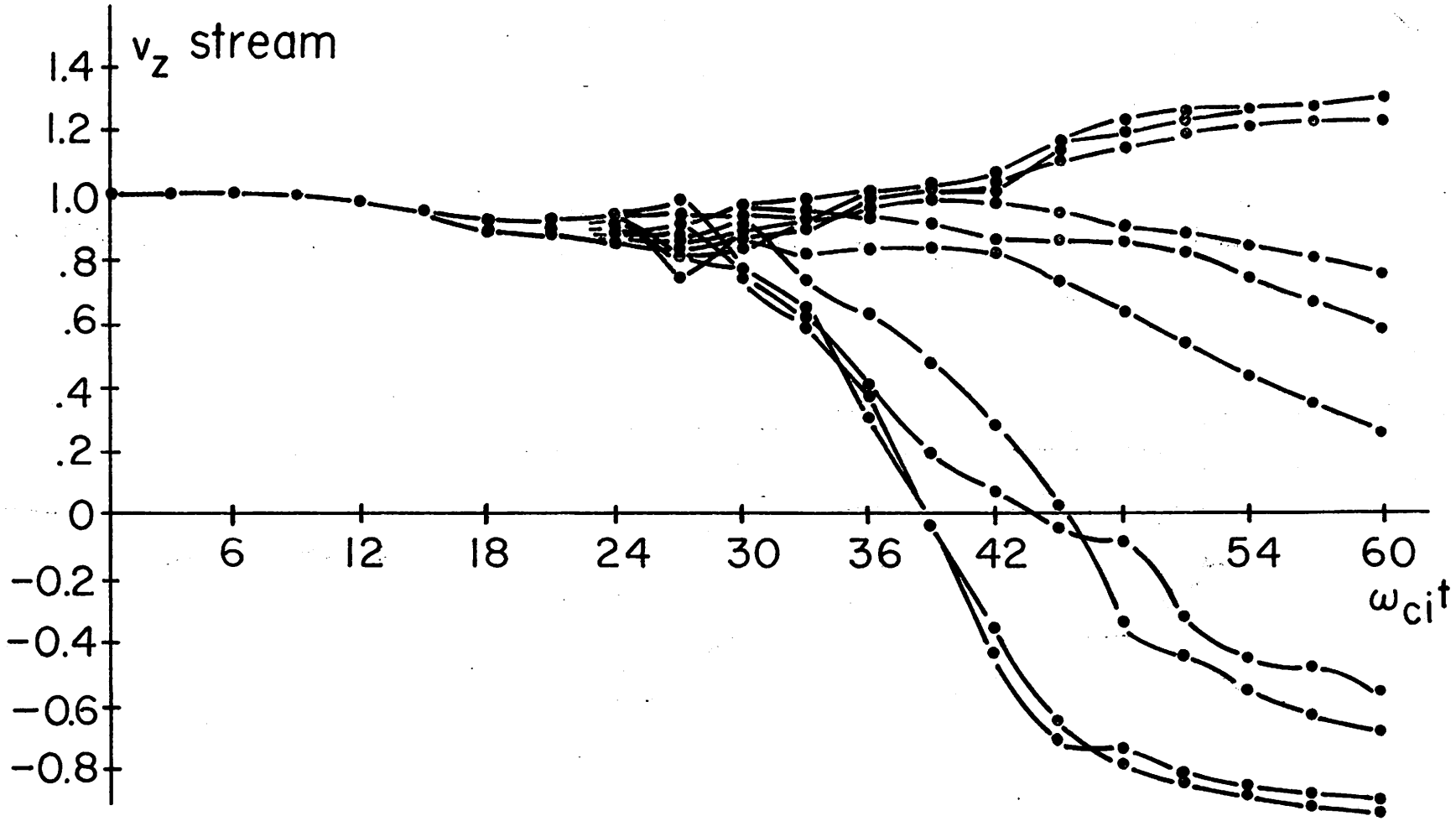
v_z stream
1.4
1.2
1.0
.8
.6
.4
.2
0
-0.2
-0.4
-0.6
-0.8
6
12
18
24
30
36
42
54
60
$\omega_{ci}t$

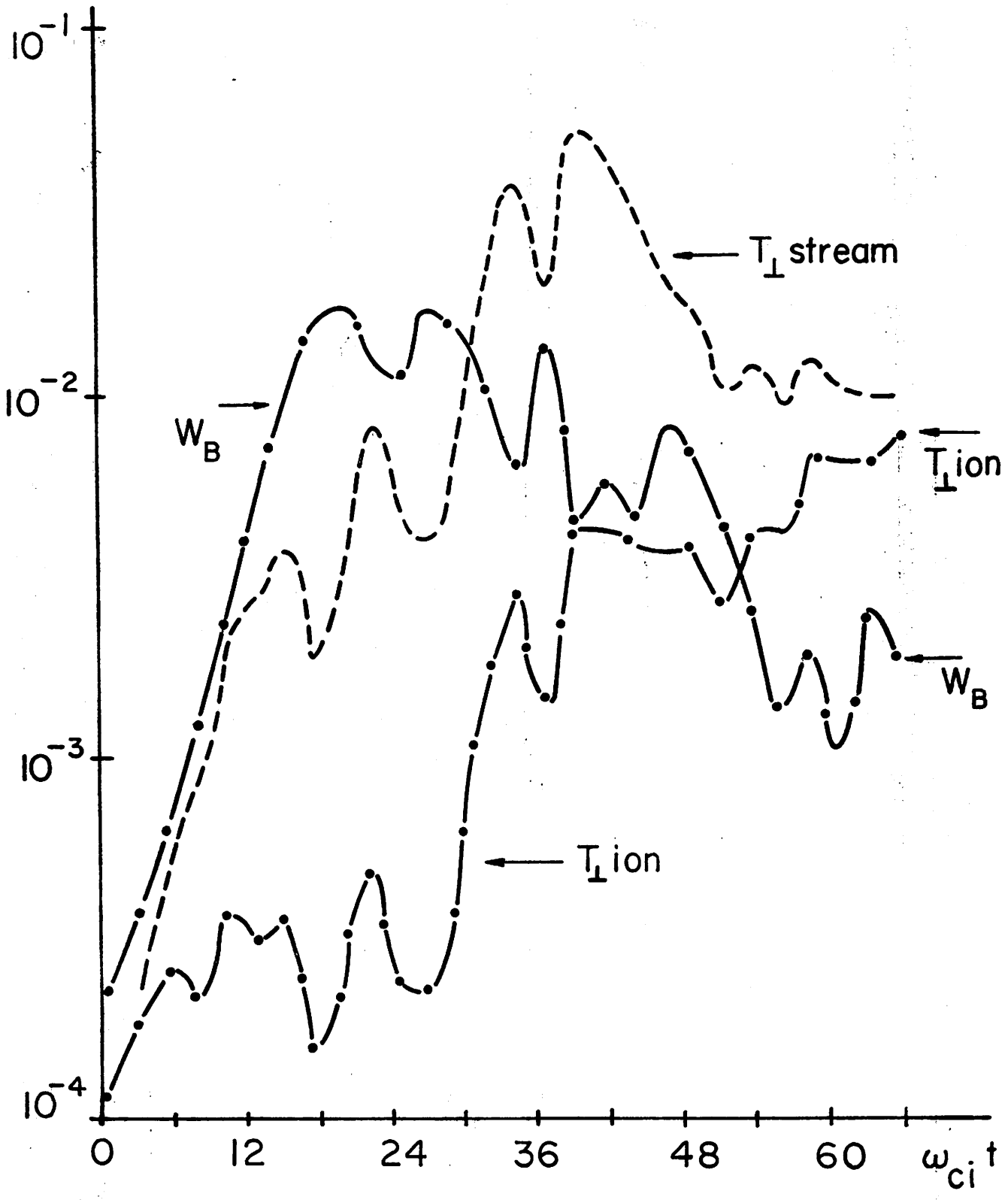
10^{-1}
10^{-2}
10^{-3}
10^{-4}
W_B
$T_\perp$ stream
$T_\perp$ ion
W_B
$T_\perp$ ion
0
12
24
36
48
60
ω_{ci} t

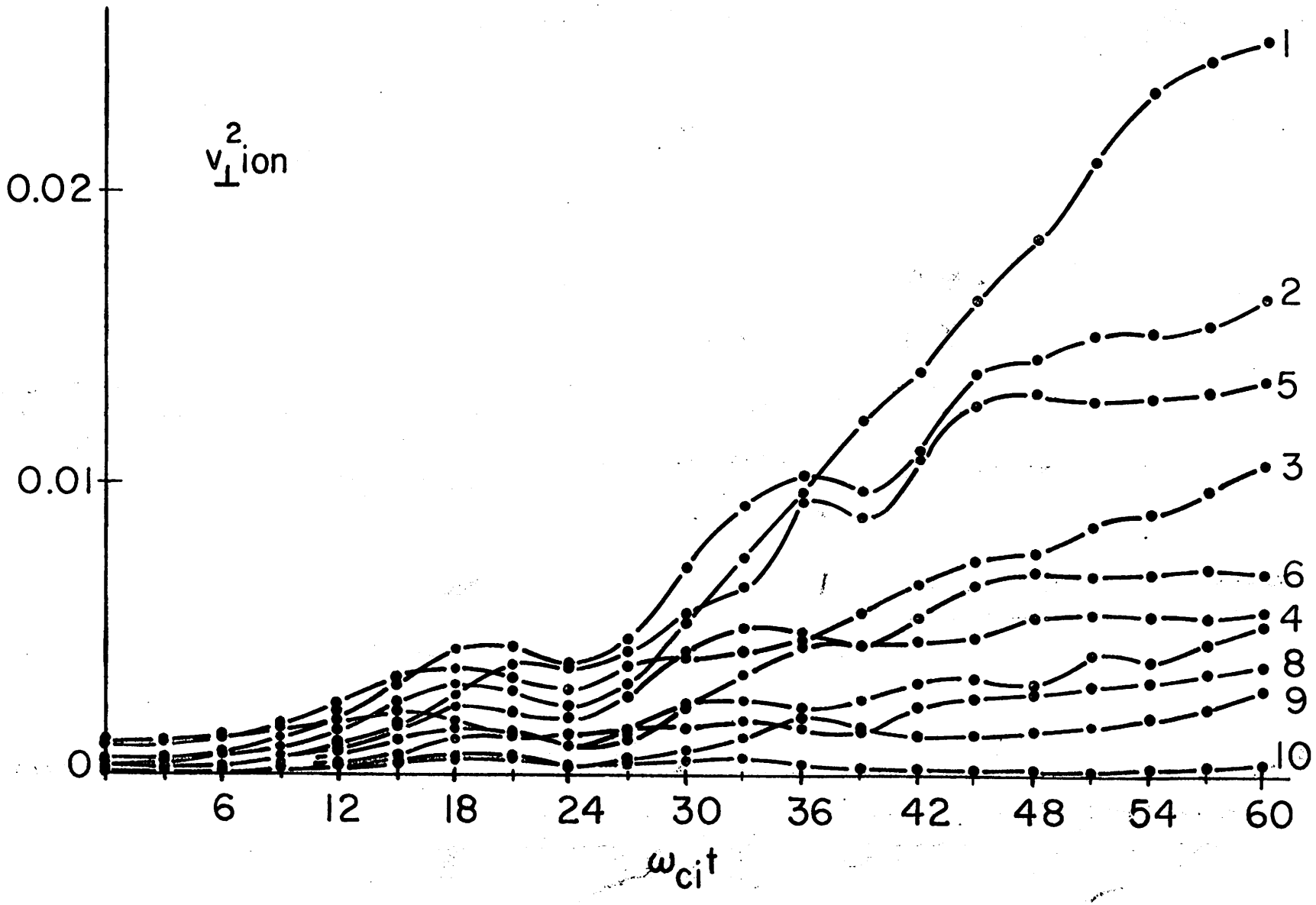
$v_{\perp}^2$ ion
0.02
0.01
0
6
12
18
24
30
36
42
48
54
60
$\omega_{ci}t$
1
2
5
3
6
4
8
9
10

TABLE I

Parameters of experiments.

Exp. No.	N	$\left(\frac{\omega_{pi}}{\omega_{ci}}\right)^2$	$k/\frac{\omega_{ci}}{c}$	$T_\perp$ initial	$T_\parallel$ initial	n_s/n_i	m_s/m_i	$\Delta t/\tau_c$
1	10	1	5.6	0	1.22×10^{-4}	---	---	0.03
2	10	1	30	4.79×10^{-4}	0	---	---	0.03
3	10 each for stream & ion	1	5.7	1.20×10^{-4} ion only	5.73×10^{-5} ion only	0.5	0.2	0.03